30-4-2019

The influence of friction parameters in a ball-screw energy-harvesting shock absorber

José Luis Olazagoitia

Lincoln Bowen

Jordi Viñolas

Nonlinear Dyn (2019) 96:2241–2256
https://doi.org/10.1007/s11071-019-04912-y

ORIGINAL PAPER

The influence of friction parameters in a ball-screw energy-harvesting shock absorber

L. Bowen · J. Vinolas · J. L. Olazagoitia

Received: 9 August 2018 / Accepted: 20 March 2019 / Published online: 30 April 2019

Abstract Energy-harvesting shock absorbers (EHSAs) have been introduced in the last decade as a viable technology for improving the performance and durability of electric and/or hybrid vehicles. However, in order to gauge the potential that can be obtained from this technology in different environments, the computational models that are used should behave as close to reality as possible. One of the limiting factors in EHSAs, in terms of recoverable energy, is frictional losses between its moving parts. Depending on the friction losses, the dynamics and efficiency of the system will vary. This paper presents a method of identifying the friction parameters in a ball-screw energy-harvesting shock absorber (BS-EHSA) system for subsequent computational simulation. In addition, it shows qualitative and quantitative results of how these friction parameters could affect the comfort and adhesion of the vehicle, as well as the generated power and energy efficiency of the BS-EHSA.

Keywords Multi-objective optimization techniques · EHSA · Energy harvesting · Electromagnetic shock absorber · Non-linearities · Vehicular dynamics · Ride comfort

L. Bowen (✉) · J. Vinolas · J. L. Olazagoitia
Departamento de Ingeniería Industrial y Automoción - D.I.I.A., Universidad Antonio de Nebrija, Madrid, Spain
e-mail: lbowen@nebrija.es

J. Vinolas
e-mail: jvinolas@nebrija.es

J. L. Olazagoitia
e-mail: jolazago@nebrija.es

1 Introduction

Hybrid and/or electric vehicles, besides being able to operate with clean energy, have the capacity to be able to count on systems that allow them to "recover" energy from different areas of the vehicle. One of the most evolutionary systems to date is the Kinetic Energy Recovery System (KERS). This technology can be encountered today in any commercial electric and/or hybrid car. Its modus operandi consists in the recovery of the kinematic energy at the moment of braking. Another technology that has made significant progress in the last decade is that of energy-harvesting shock absorbers (EHSAs). These systems replace conventional shock absorbers, and their damping effect is provided by the electromagnetic torque of a generator, while at the same time generating electrical power.

There are multiple EHSA proposals available in the pertinent literature on this subject. Among them are those that work with a linear generator [20,28,38] and/or those that work with a rotational generator [2]. As the movement in most conventional shock absorbers is a translation, the use of rotational generators requires a translation–rotation transmission system. Several options are available: the ball-screw mechanism (BS-EHSA) [1,17,19,29], the rack pinion mechanism [10,13–15,34], the hydraulic transmission

[7,8,16,21,31,33], the algebraic screw linkage [24] and/or the two-leg motion conversion [18].

Most of the EHSA systems presented in published studies have not been installed in a real car. For that reason, computational models are needed in order to study not only the vehicle dynamics, but the energy-harvesting potential. Those computer models must be able to encompass the largest possible number of parameters, in such a way that they can replicate the behavior of the real system. One of the limiting factors in EHSAs, in terms of recoverable energy, is the frictional losses between its moving parts. Depending on these frictional losses, the dynamics and efficiency of the system will change. Modeling these friction phenomena requires performing experiments and methods of identifying nonlinear parameters.

Friction is present in suspension components in different levels. In some cases, friction is used as the main factor to provide damping. This is the case of suspensions based on leaf springs or suspension components of freight wagons. One advantage of such friction components is that they are relatively cheap and almost maintenance- free. Additionally, the amount of damping is such that it can be made proportional to the axle load. However, the disadvantage is that the efficiency of friction dampers depends on parameters that are normally out of control of the designer (especially if there are wear and aging effects): the friction coefficient in the contacting surfaces and the flexibility of the arrangement. This means that the dynamics can be highly affected and that this uncertainty becomes a challenge for dynamic simulations of vehicles which, to a great extent, rely on friction damping [11]. In other cases, friction damping is only a side effect; such is the case of rubber parts used thoroughly in suspensions or air springs. Modeling in this case requires a different approach, and a good survey can be found in [5].

The identification of nonlinear dynamic parameters has been studied by many authors in different areas. As far as the suspension systems are concerned, Zhang et al. [30] propose the identification of nonlinear parameters from a shock absorber that works by means of magnetic effects; Zhu et al. [35] identify the nonlinear parameters of an air spring with a shock absorber at high and low amplitudes. With regard to friction phenomena, Kashani [12] studies the hysteresis phenomena produced by friction forces, and Vidmar et al. [25] study the effect of the Coulomb friction on the performance of centrifugal pendulum vibration absorbers.

The two main characteristics that most of the authors focused on when they are designing an EHSA are: the power generated and the damping force. With regard to the first point, the literature provides numerous works which estimate the power that can be obtained with the EHSA under different conditions (travel speeds, road profiles or excitation frequencies) [26,27,32]. However, the results shown are only theoretical without taking into account the influence that frictions can have on the system. On the other hand, concerning the damping force, the presence of nonlinear friction forces in the EHSA affects the vehicle dynamics, especially comfort and ride handling, as Benini et al. analyzed [3].

This article seeks to demonstrate the importance that the parameters of friction in the EHSA systems can have, both in the vehicle dynamics and in the efficiency for the recovery of energy. For this, a qualitative and quantitative analysis of the friction parameters in the dynamic and energetic behavior of these technologies is carried out. This work focuses on the operating principle of the BS-EHSA system, in which a computational model is developed in Simscape/Mathworks. Then, with the help of experiments in a bench test, its friction parameters are identified.

The article is divided into 5 sections. The second section describes the manufactured prototype of the BS-EHSA, along with its computer model and the experimental tests carried out. The third section shows first the procedure followed to obtain the nonlinear friction parameters and then the values of the estimated friction parameters. In the fourth section, in order to analyze the influence of friction parameters, two types of studies are carried out. The first study is done using the design parameters of the manufactured prototype of the BS-EHSA and taking into account the damping curves. Meanwhile, for the second study an optimization of the BS-EHSA system is performed, and once optimized, the impact of the frictions is analyzed. For both studies, numerical results are given. In Sect. 5, the salient outcomes from this study are summarized.

2 Prototype, computational model and experimental setup

Among other possible design options, the BS-EHSA has been chosen to analyze the importance of friction in

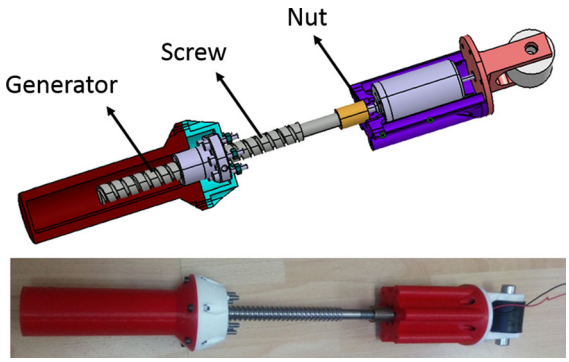

Fig. 1 Top: cad model of a ball-screw energy-harvesting shock absorbers (BS-EHSA). Bottom: photograph of the BS-EHSA prototype

Table 1 Main characteristic of the BS-EHSA

Inertia of motor	J_m	121	g cm^2
Inertia of screw	J_s	180	g cm^2
Screw lead	τ	5	mm/rev
Resistance of the generator	R_i	6.6	Ω
Voltage constant	K_{re}	0.137	Vs/rad
Torque constant	K_t	0.137	Nm/A
Inductance of the generator	L_i	1.7	mH

the energy-harvesting shock abosrbers (EHSAs). The BS-EHSA uses a transmission ball screw which enables us to convert the translation movement that we find in conventional dampers to a rotating movement. Therefore, a rotating generator is connected, so that the resistant electromagnetic torque is the one that will give us the damping force, while in turn generating energy. In Fig. 1a, prototype can be observed. In Table 1, the design parameters of this shock absorber are specified. It has been decided to use the BS-EHSA system because it is one of the technologies of energy recovery dampers with the least friction compared to others (e.g., rack pinion [15], hydraulic [36] and/or two-leg mechanism [18], etc).

The BS-EHSA analysis will be carried out by coupling it in a model of a quarter car (see Fig. 2) where m_2 and m_1 correspond, respectively, to the suspended and unsuspended mass, k_2 and k_1 represent the stiffness of the suspension and the tire, and m_{eq}, c_{eq} and k_{eq} are the parameters of the equivalent mechanical system of the BS-EHSA, previously derived by Bowen et al. [4]:

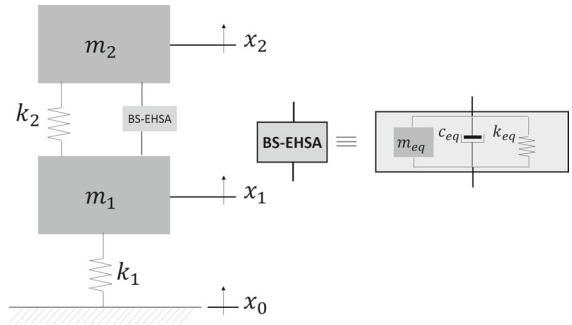

Fig. 2 BS-EHSA incorporated in a quarter car model and its equivalent mechanical system configuration

$$m_{eq} = \frac{J_m + J_s}{\tau^2} \tag{1}$$

$$c_{eq} = \frac{K_t K_{re}(R_e + R_i)}{\tau^2((R_e + R_i)^2 + {L_i}^2\omega^2)} \tag{2}$$

$$k_{eq} = \frac{K_t K_{re} L_i \omega^2}{\tau^2((R_e + R_i)^2 + {L_i}^2\omega^2)} \tag{3}$$

The equivalent mass m_{eq} not only depends on the inertia of the screw J_s and the motor J_m, but also on the screw lead τ. On the other hand, the c_{eq} and k_{eq} depend on the electrical resistance (R_{tot}), of the generator (R_i) and the external load connected (R_e), the generator inductance L_i, the torque constant K_t, the voltage constant K_{re}, the excitation frequency of the system ω and also the screw lead τ. It is important to remark that the screw lead and the screw diameter d_s compromise the efficiency η_{bs}—of the ball screw. In this way, the damping force provided by the BS-EHSA is equal to:

$$f_d = m_{eq}(\ddot{x}_2 - \ddot{x}_1) + c_{eq}(\dot{x}_2 - \dot{x}_1) + k_{eq}(x_2 - x_1) + \tau_{fbs} + \tau_{fsm}/\tau \tag{4}$$

The terms τ_{fbs} and τ_{fsm} represent the friction parameters that influence the behavior of the system. The first term is the friction between the nut and the screw, while the second has to do with the bearings of the generator (see Fig. 3). The friction models used are the same as those presented by Xie and Wang [27] (see Fig. 4).

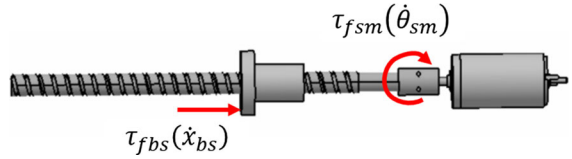

Fig. 3 BS-EHSA schematic including the friction parameters

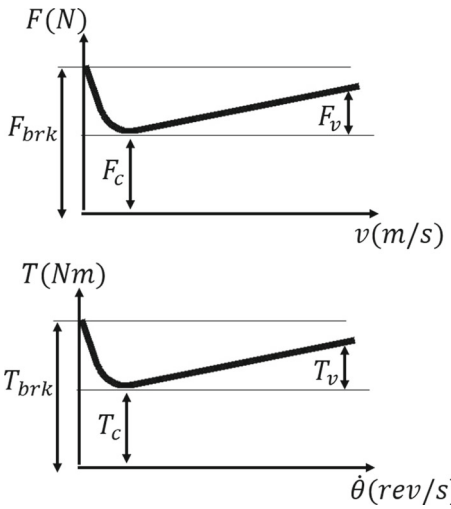

Fig. 4 Function of the translational friction (up) and rotational friction (down)

3 Friction parameters

This section details the experiments that were carried out and the method used to identify the friction parameters.

3.1 Identification of the dynamic parameters

The BS-EHSA prototype was tested on a MTS 835 machine (see Fig. 5). Tests were carried out at different excitation frequencies (0.5–3.5 Hz), all with an amplitude of 15 mm. In addition, for each excitation frequency, different electrical resistances (15, 47 and 109) were connected to the generator.

From each test, the damping force exerted by the BS-EHSA and the voltage coming from the generator are recorded. The damping force together with the excitation speed is given by the MTS 835 machine, and the voltage is acquired through the NI cDaq-9178 system together with the NI 9234 module. These experimental results are used to compare them with the simulation results and estimate the friction parameters that best suit the behavior of the system.

Figure 6 shows the computational model of the BS-EHSA prototype installed in the MTS 835. The program that is used to simulate the behavior is Simscape/Mathworks. The model contains: the system input (number 1) that will be the displacement that we indicated with the MTS-835, the sensor to measure the input force (number 2) that is already incorporated in the machine, the friction between the nut and the screw (number 3) and on the generators bearings (number 4), the system to acquire the generator voltage (number 5) and finally the BS-EHSA system together with its inertias (number 6).

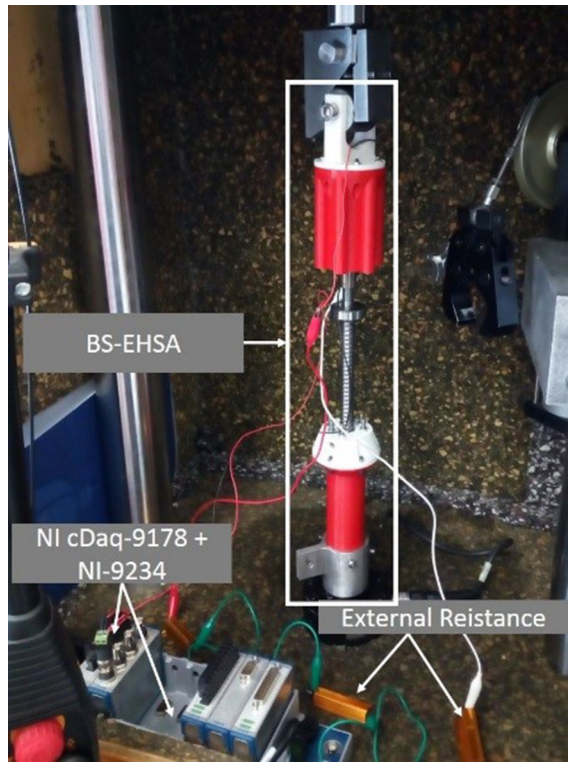

Fig. 5 Bench test for the BS-EHSA

In order to obtain the friction parameters, both the experimental tests and the computational model presented in Fig. 6 are used. Due to the difficulty in finding the exact friction values that exist in the BS-EHSA system, it has been decided to establish upper and lower bounds that allow us to determine the range in which these parameters can be found.

The procedure (Fig. 7) followed to obtain the upper and lower bound for each friction parameter ($\overrightarrow{F_r}$) is as follows:

1. From the tests carried out on the MTS-835, at different excitation frequencies (ω) and external loads (R_e), the experimental data of the generator voltage V_e, the input force F_e and the input displacement x_0 are obtained,

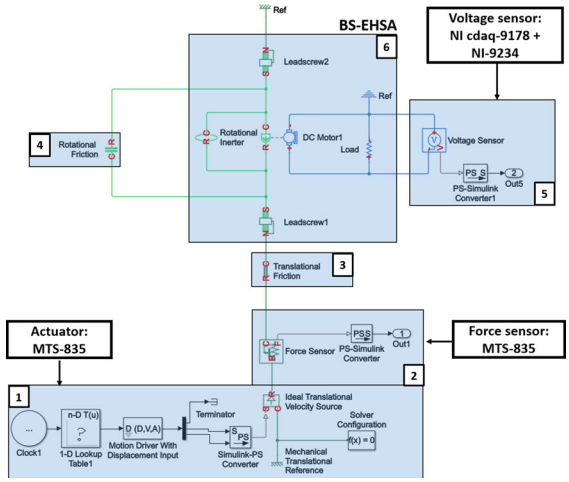

Fig. 6 Simscape/MATLAB model of the BS-EHSA test bench

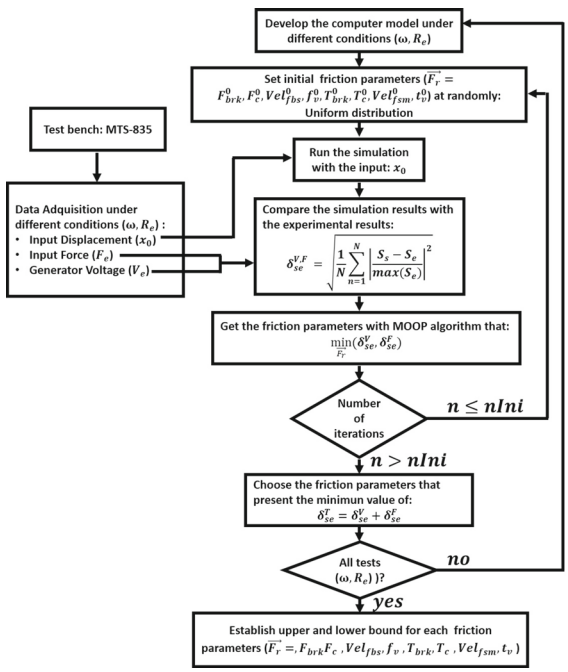

Fig. 7 Scheme for find the friction parameters of the model

2. On the other hand, the computational model is developed in Simscape/Mathworks (Fig. 6) with the specifications of mass and external resistance for each test. The values of the initial friction parameters ($\overrightarrow{F_r} = F^0_{\text{brk}}, F^0_{\text{c}}, \text{Vel}^0_{\text{fbs}}, f^0_v, T^0_{\text{brk}}, T^0_{\text{c}}, \text{Vel}^0_{\text{fsm}}, t^0_v$) are taken randomly using a uniform distribution, among the possible values given by the distributor,
3. With the data of the input offset x_0, obtained from the bench test, the simulation is executed, in which the information of the generator voltage V_{s} and the input force F_{s} is obtained,
4. the two simulation signals (V_{s}, F_{s}) with the two experimental signals (V_{e}, F_{e}) are compared, and a scalar for each one (δ^V_{se}, δ^F_{se}) is deduced. To obtain the scalar, the following equation is used 5:

$$\delta_{\text{se}} = \sqrt{\frac{1}{N}\sum_{n=1}^{N}\left|\frac{S_{\text{s}} - S_{\text{e}}}{\max(S_{\text{e}})}\right|} \tag{5}$$

5. With the aid of a multi-objective optimization algorithm (MOOP), the objective is to minimize the two scalar values (δ^V_{se}, δ^F_{se}) by varying the friction parameters ($\overrightarrow{F_r}$). In this case, the MATLAB function: fminimax is used, which is based on the algorithm of Brayton et al. [9],
6. Repeat the simulation for different initial friction parameters, up to a total of $nIni$ initial conditions,
7. Once the MOOP algorithm is concluded, the convergence point is noted, and the friction values that allow a lower value of the resulting scalars (δ^V_{se}, δ^F_{se}) are chosen,
8. The procedure described so far will be repeated for each of the tests. In this way, it is ensured that the friction parameters are independent of the resistance that is connected to the generator and the excitation frequency of the BS-EHSA. Once the values of the friction ($\overrightarrow{F_r}$) are obtained for each test (ω, R_{e}), the maximum and minimum values of these are chosen and established as the upper and lower bounds.

It should be pointed out that the reason the model is simulated with different starting points is because the problem that is being solved has non-linearities, and the MOOP algorithms remain trapped in local minimums.

3.2 Friction parameters values

The MOOP algorithm used in this work enables to reduce the difference between the experimental and simulation results for the two objective functions (δ^V_{se}, δ^F_{se}) simultaneously. An example is shown in Fig. 8: the value of the two scalars decreases in each iteration by varying the values of the friction parameters, see Fig. 9. Figure 10 shows an example of how changing a friction parameter (t_v in this case) decreased the total

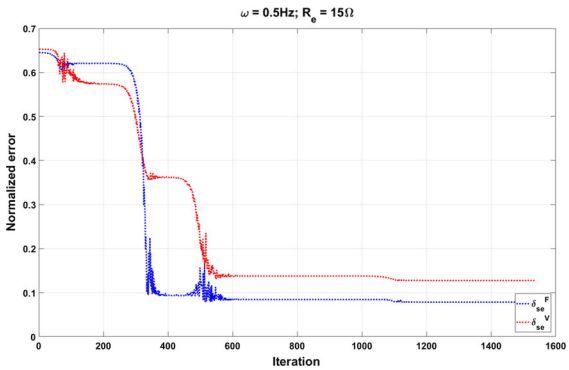

Fig. 8 Scalar values of the objective functions at each iteration that represent the normalized error between the experimental and simulation results

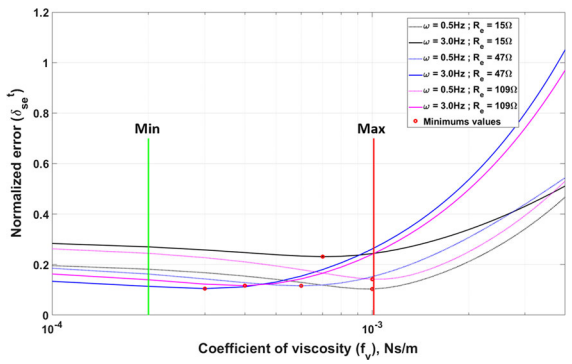

Fig. 10 Example of a nonlinear dynamic behaviors from the viscous coefficient rotational parameter (t_v). In the figure are indicated the values of the friction parameter, for different tests, that allow to reduce the difference between the experimental and simulation results ($\delta^t_{se} = \delta^F_{se} + \delta^V_{se}$)

error (δ^t_{se}). Showing in the first place, why maximum and minimum boundaries for every friction parameter were set. And in the second place, why the identification of the friction parameters has been focused as a nonlinear problem identification.

An example of the fit between test and model is shown in Fig. 11. Here, it can be seen how there is a correlation between the experimental and simulation values, with the results of one approximating closely to those of the other. It should be mentioned that in the graphs of the input force and voltage of the generator there are small peaks in the experimental data that surpass the simulation data. This is

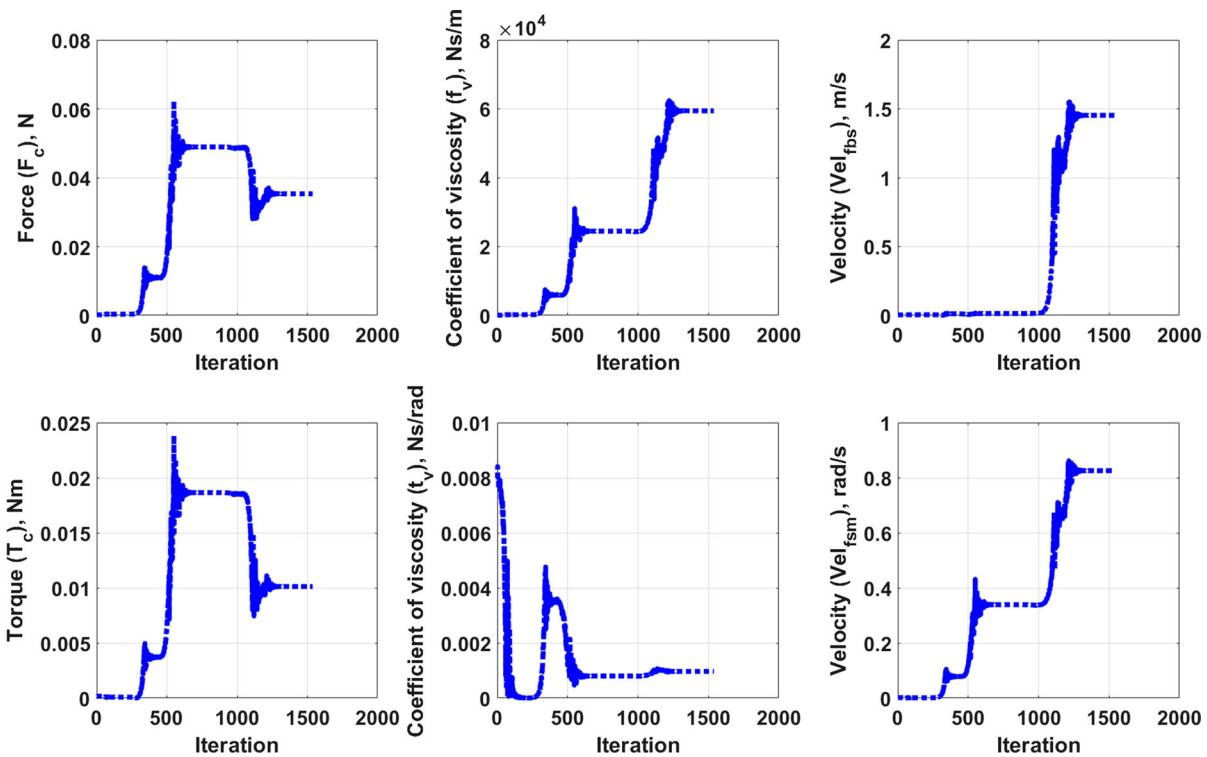

Fig. 9 Values of the friction parameter at each iteration in the MOOP algorithm from the test ($\omega = 0.5$ Hz; $R_e = 15\,\Omega$)

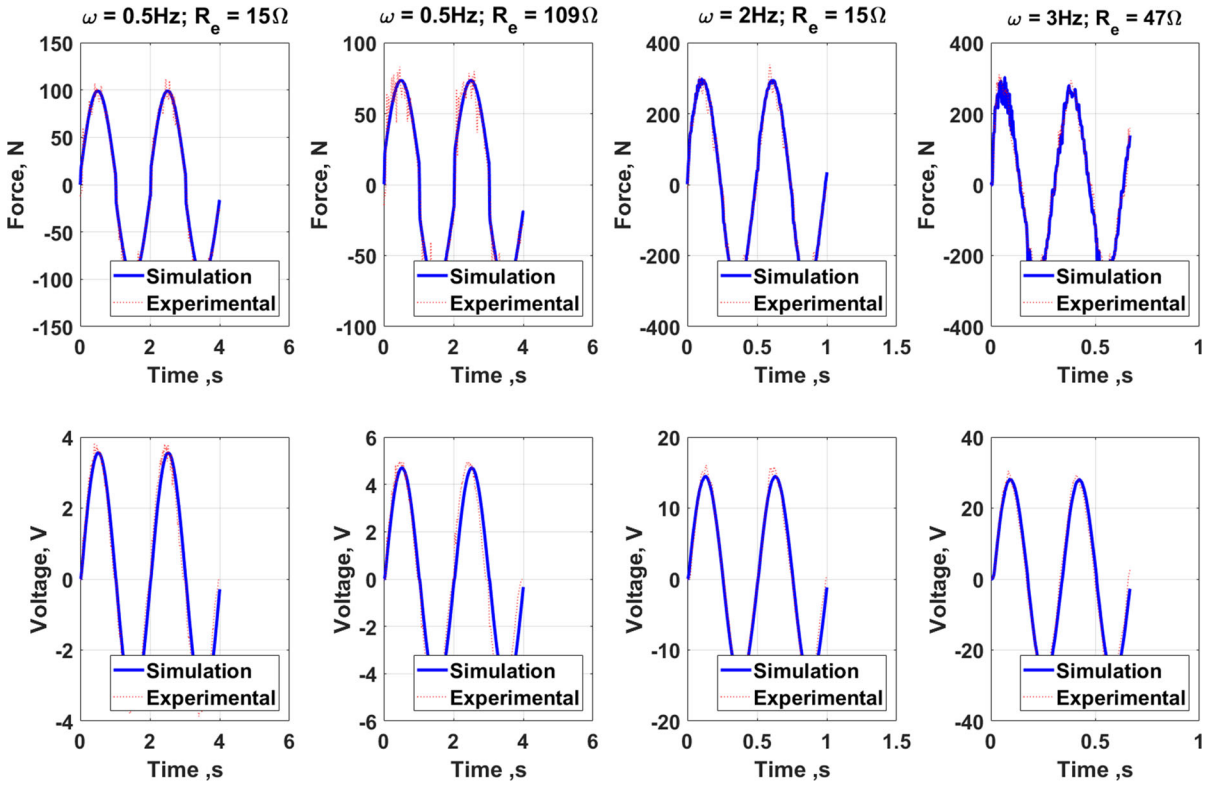

Fig. 11 Results of the input force and generator voltage from different tests using the MOOP algorithm

Table 2 Friction parameter values (maximum and minimum values)

		Max	Min
Coulomb translation friction force, F_c	N	144.90	0.014
Breakaway translation friction force, F_{brk}	N	145.80	0.017
Viscous coefficient translation friction, f_v	Ns/m	59,420	7049
Breakaway friction velocity, Vel_{fbs}	m/s	492.28	0.104
Coulomb rotational friction torque, T_c	Nm	0.057	0.0053
Breakaway rotational friction torque, T_{brk}	Nm	0.058	0.0065
Viscous coefficient rotational friction, t_v	Ns/rad	0.001	1.012e−4
Breakaway friction velocity, Vel_{fsm}	rad/s	489.67	0.0164

because the created computed model does not contemplate the effects of backlash between its moving parts.

The numerical values of the friction parameters are shown in Table 2 and Fig. 12. As indicated above, from the results of all the experimental tests, the maximum and minimum values of each friction parameter were established as their maximum and minimum bounds.

4 Influence of the friction parameters

This section analyzes the influence of the friction parameters, calculated in the previous section, on the dynamic behavior of the quarter car model (Fig. 2) and on the power generation of the BS-EHSA. For this, two studies will be carried out. The first is done using the design parameters of the manufactured BS-EHSA prototype and taking into account the damping curves.

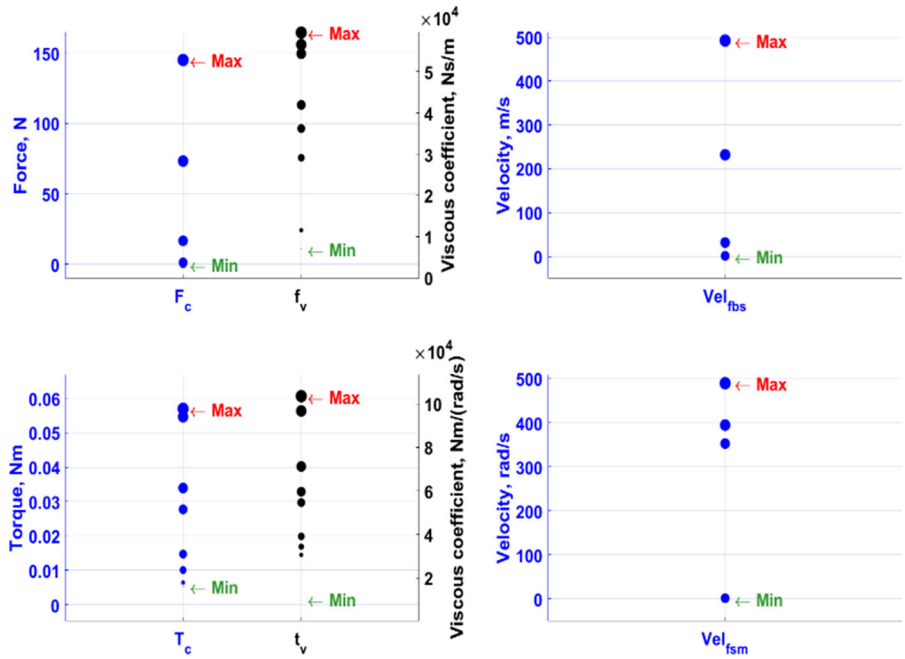

Fig. 12 Maximum and minimum values of the friction parameters. Calculated from all the experimental and simulation results

While for the second study, first an optimization of the BS-EHSA system is performed, and once optimized, the impact of the frictions is analyzed

4.1 Prototype of the BS-EHSA

One of the main characteristics of the electromagnetics EHSAs is that their damping coefficient (c_{eq}) varies according to the external resistance that is connected to the generator. As deduced from Eq. 2, the coefficient is inversely proportional to the value of the electrical resistance (R_e). Consequently, the greater damping value that can be obtained from an EHSA, without changing its design parameters, is when the generator is in short circuit ($R_e \approx 0$). Likewise, the lowest damping value is obtained at the moment in which the generator is in open circuit ($R_e \approx \infty$).

The electrical resistance that is connected to the generator is chosen according to the damping curve that is required for the vehicle where the EHSA will be installed. However, the internal friction forces of the system can greatly influence the value of the absolute damping coefficient of the EHSA.

The EHSAs are systems to work in a far wider frequency band than the range between 5 and 8 Hz, which is used for the system described in the article of Erturk and Inman [6]. This is because the irregularity of the road surface is a stochastic quantity and that the driving velocity is arbitrary within a certain range. Although it is true that when the vehicle is in one of its modes of vibration the level of voltage generated increases, the main purpose of these systems is to provide a sufficient damping and thereby a good dynamic behavior of the vehicle in all operating scenarios. Compared to this, the energy harvesting is a secondary aspect.

Figure 13 shows that depending on the magnitudes of the values of the friction parameters, the voltage of the BS-EHSA varies. At lower friction, the resonance peaks are more damped; as the displacement of the suspended mass decreases further, the voltage level decreases. The figure shows how the friction parameters affect the generation of voltage for different electrical loads connected to the generator. The non-smooth characteristics of dry friction and its impact on a systems dynamic behavior are a topic, which has been investigated and discussed for a long time. In fact, such systems can be highly sensitive even to small changes of the parameters. Furthermore, the modeling of the friction itself including the transition between the states of adhesion and sliding is a rather wide field. Just one example for such investigations is the works by Popp [22,23] and his co-workers on friction oscillators. In the present work, the non-smooth characteristics of friction do not seem to be an essential effect and measurements

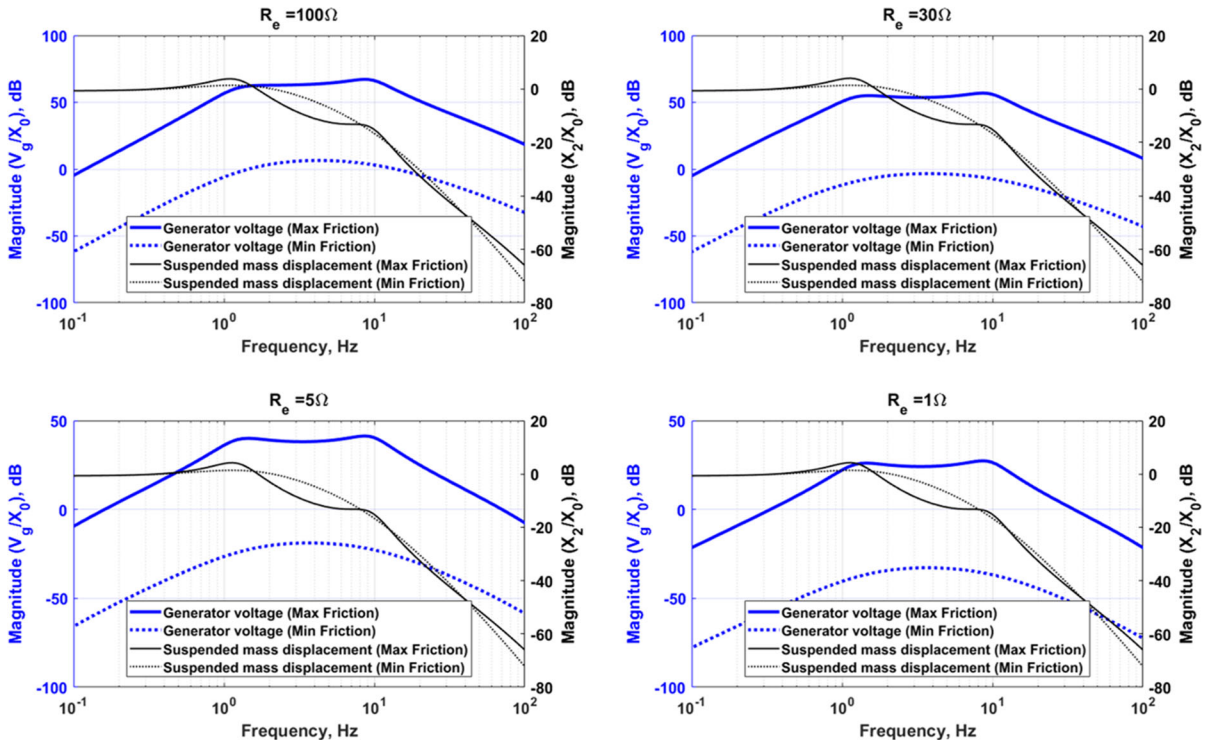

Fig. 13 Generator voltage (V_g) frequency response from the BS-EHSA installed in a quarter car model and the suspended mass displacement (x_2) frequency response. Both are showed with minimum and maximum values of friction and different external loads (R_e) connected to the generator

did not indicate an impact of the dry friction in the way of a radical altering of the systems behavior, e.g., varying periodicity.

In Fig. 14, the damping curves are shown when the generator is in open circuit and short circuit. In green, the curves correspond to the minimum values of friction, while the red ones the maximum values of friction. The graph shows that the damping coefficient, for the case of open circuit, can go from 293 to 2306 Ns/m, depending on the friction values that the system has. While in the case of short circuit, the value of the coefficient can go from 2862 to 6208 Ns/m.

Figure 15 is composed of four figures. Figure a) corresponds to the PSD of the signal used as input to the quarter car model. In this case, there is a standardized road profile type C. Figure b) shows the displacement of the suspended mass and the RMS values of the suspension velocity. It should be point out that the values of the RMS velocities, taking into account either maximum or minimum values of the frictions, are on the range tested in Sect. 3 ($0.5\ \text{Hz} < \omega < 3.5\ \text{Hz}$

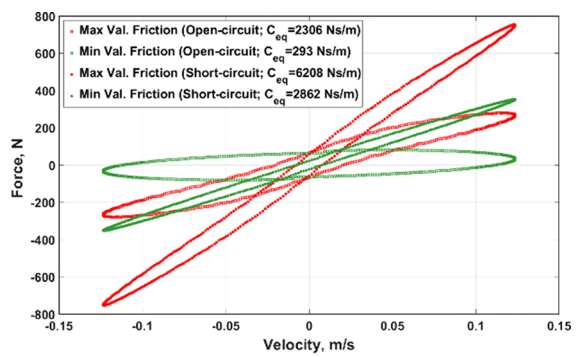

Fig. 14 Force–velocity curve of the BS-EHSA, when the generator terminals are in short circuit and open circuit, using the maximum and minimum friction parameters

and Amplitude = 15 mm); Fig. 16 shows more clearly the main excitation frequencies that intervene in the suspension. Figure c) shows the instant power generated. For both cases, the BS-EHSA system is compared with frictions, taking into consideration the maximum and minimum values, and without them. Finally, fig-

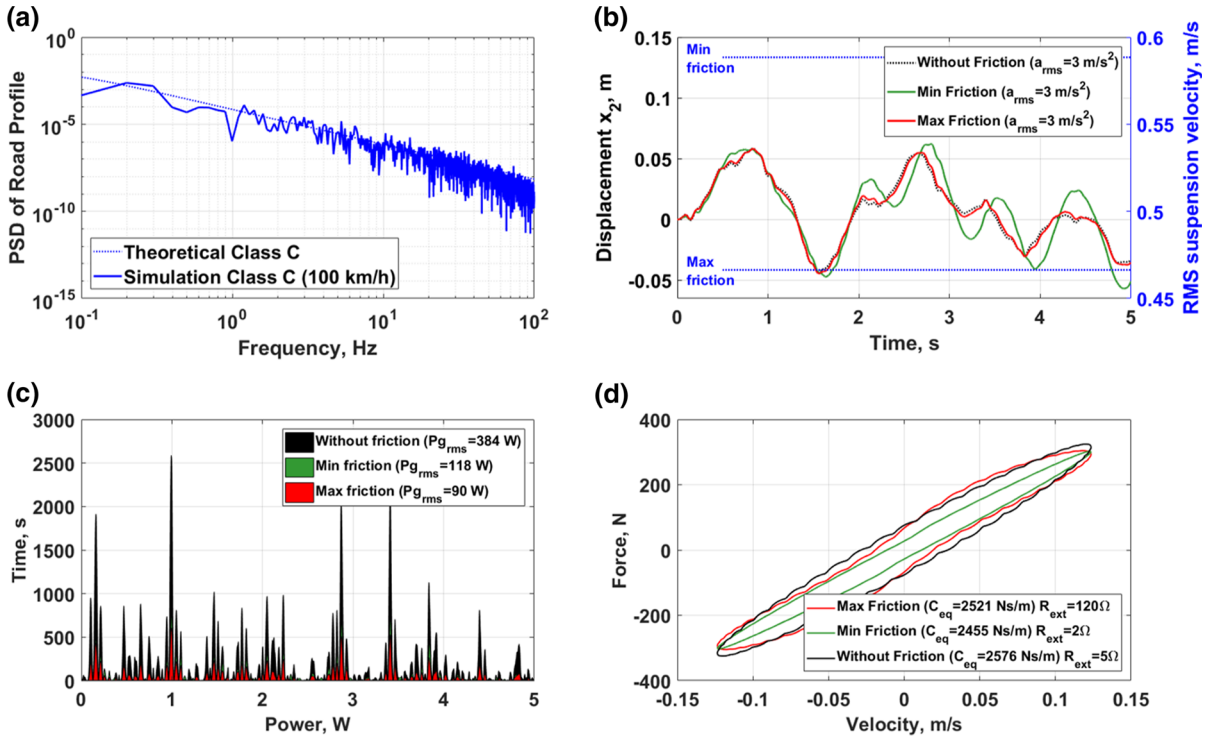

Fig. 15 **a** Logarithmic PSD of the road profile; **b** displacement of the suspended mass; **c** power recovered from the BS-EHSA, without friction, with minimum values of friction and with maximum values of friction; **d** force–velocity curve of the BS-EHSA without friction, with minimum values of friction and with maximum values of friction

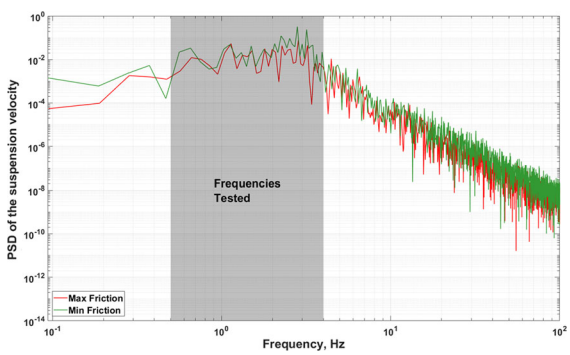

Fig. 16 PSD of the suspension velocity from a single-seater vehicle driven in a road class C profile at 100 km/h

ure d) shows the damping curves for the three cases studied (maximum, minimum and frictionless values). The values of the external load are adjusted in such a way that the damping coefficients, or what is the same, the slopes of the force–velocity curve resemble each other.

In this way, we can compare the three cases starting from the condition that the three systems have the same damping curve. As can be seen from figure c and due to friction, the average power generated can be reduced between 70 and 80%, compared to a frictionless system. On the other hand, the comfort of the system, since all three have the same damping curve, does not undergo significant changes. Showing in b, the suspended mass does not undergo a change in its average acceleration ($3\,m/s^2$) comparing the three cases.

4.2 Optimization of the BS-EHSA

The influence of the friction parameters in an optimized BS-EHSA system is analyzed qualitatively and/or quantitatively in this section. The optimization will be done using the system of two degrees of freedom (quarter car) and without taking into account friction parameters. The optimized BS-EHSA, besides guaranteeing comfort and stability in the car, should be able

Table 3 Maximum and minimum values of the optimization variables

Variables	Max	Min	
Total inertia, $J_t = J_m + J_s$	10,000	250	g cm^2
Screw lead, τ	20	5	mm/rev
Voltage constant, K_{re}	11,900	29.8	rpm/V
Resistance of the external load, R_e	10,000	1	Ω

to recover the maximum amount of energy and also be efficient. Therefore, four types of objectives must be considered:

1. Minimize the average acceleration of the suspended mass; less acceleration greater comfort.
2. Minimize the relative displacement between the wheel and the ground surface; less displacement greater vehicle adhesion.
3. Maximize the power generated by the BS-EHSA.
4. Maximize the energy efficiency, efficiency being the ratio between the energy generated and the damped energy.

In order to handle dimensionless variables, the following expressions are used:

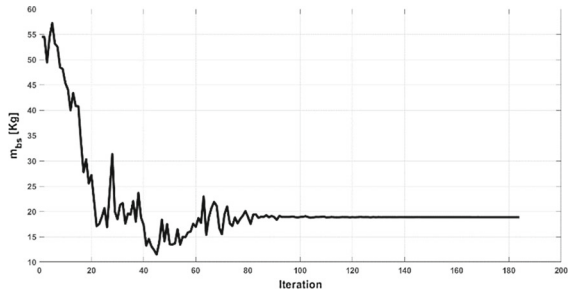

Fig. 18 Values of equivalent mass m_{eq} from BS-EHSA at each iteration

$$\alpha_{w,\mathrm{rms}} = \frac{\mathrm{rms}(w(s)\ddot{x}_2)}{g} \tag{6}$$

$$\eta_{\mathrm{rh}} = \frac{k_1(x_1 - x_0)}{g(M_1 + M_2)} \tag{7}$$

$$\rho_g = \frac{V_g^2}{g(M_1 + M_2)R_e V_t} \tag{8}$$

$$\eta_g = \frac{V_g^2}{R_e c_{eq}(\dot{x}_2 - \dot{x}_1)^2} \tag{9}$$

where $\alpha_{w,\mathrm{rms}}$ represents the dimensionless comfort, which is achieved by filtering the acceleration of the suspended mass $\ddot{x}_2$, using the filter $w(s)$ proposed by Zuo et al. [37], and dividing by the gravity. The η_{rh} represents the cars adhesion to the ground in a

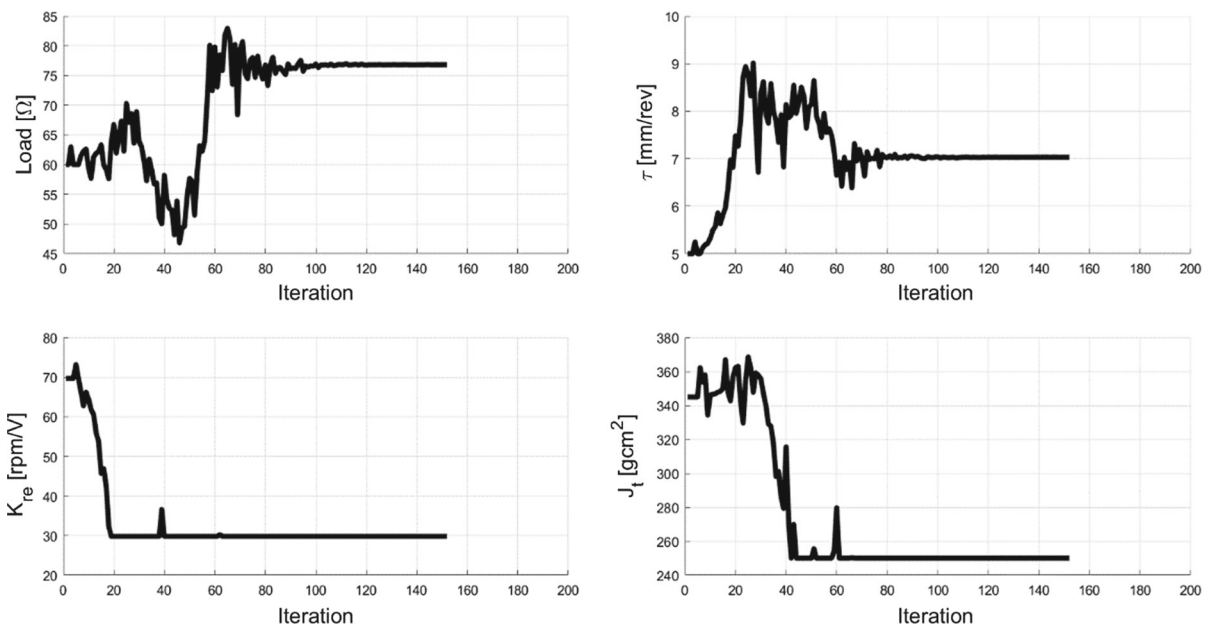

Fig. 17 Values of the design parameters of the BS-EHSA at each iteration: external load R_e, screw lead τ, voltage constant K_{re} and total inertia $J_t = J_s + J_m$

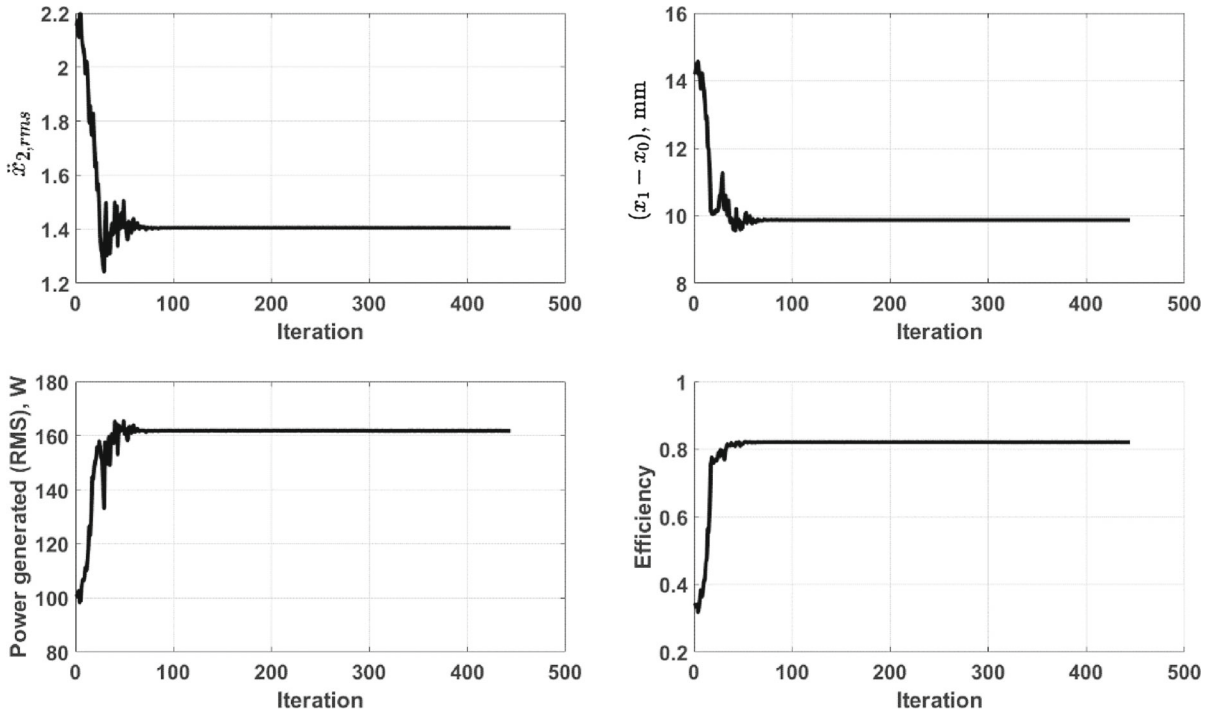

Fig. 19 Results of the parameters: comfort, road handling, power generated and efficiency

dimensionless way [10] and comprises the displacement difference between the non-suspended mass x_1 and the ground x_0, multiplied by the stiffness of the wheel k_1 and divided by the sum of the suspended mass M_2 and non-suspended mass M_1 all multiplied by the gravity. The ρ_g represents the electrical power generated in a dimensionless way which is composed of the voltage on the generator V_g squared, divided by the sum of the masses multiplied by the gravity, the electric resistance and the car speed V_t. The η_g, which indicates the efficiency of the EHSA, represents the amount of energy that is recovered with respect to the energy that is used to damp. For that reason, it is composed of the electric power divided by the damped power.

For the optimization of the BS-EHSA, we used the fgoalattain algorithm and the variables of: external electrical resistance R_e, the screw lead τ, the total inertia ($J_t = J_m + J_s$) and the electromagnetic constant of the generator K_{re}. With the objective function:

$$\min_{\vec{x}=R_e,\tau,J_t,K_{re}} f(\vec{x}) = \left[\alpha_{w,\mathrm{rms}};\ \eta_{\mathrm{rh}};\ \frac{1}{\rho_g};\ \frac{1}{\eta_g}\right] \quad (10)$$

Therefore, our objective function is to minimize the average acceleration and the relative displacement between the ground and the wheel and in turn maximize the amount of power generated and its efficiency. The procedure used to optimize it is as follows: firstly, with the PSD (power spectral density) of a class C road, driving at a speed of 70 km/h, the input to the system x_0 is obtained. This input is entered into the quarter car computer model, with the initial design values that are used in the test bench. This model gives as output values the dimensionless parameters: $\alpha_{w,\mathrm{rms}}$, η_{rh}, ρ_g and η_g, which is part of the objective function previously mentioned. The variables that are used to optimize the BS-EHSA were set at higher and lower levels, depending on market availability. These maximum and minimum values are shown in Table 3.

Figure 17 shows the values of the variables in each iteration until their convergence. The final value for the total inertia J_t is 250 g cm^2, and the generator voltage constant is 29.8 rpm/V; both correspond to their lower boundary dimensions. The value of the screw lead is 7 mm/rev, and the final value of the electrical resistance that is connected to the generator is 75 Ω. It is important to note that although the inertia value increases, the equivalent mass at each iteration decreases (see Fig. 18), because the screw lead increases (see Eq. 2).

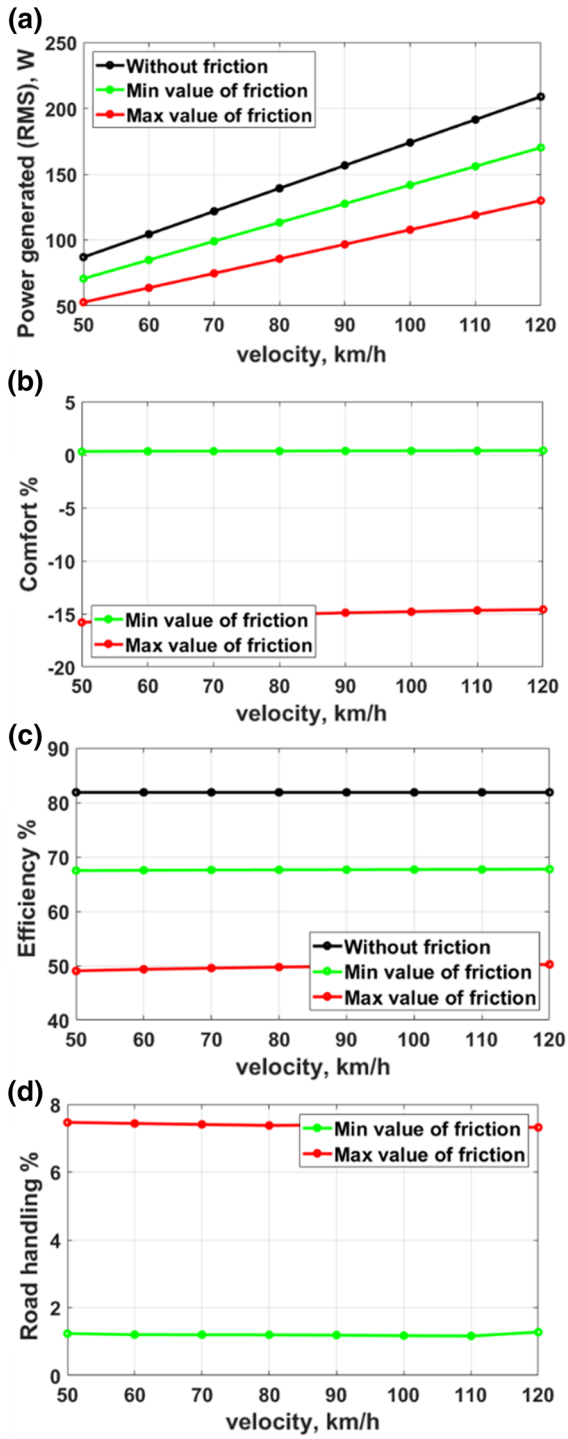

Fig. 20 **a** Power generated; **b** percentage of comfort compared to the system without friction; **c** efficiency; **d** percentage of road handling compared to the system without friction—all of these at different vehicle speeds

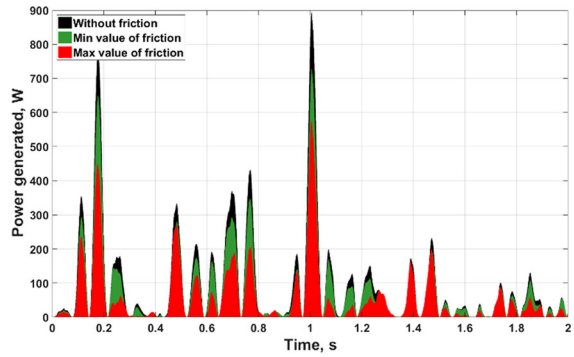

Fig. 21 Power recovered from the BS-EHSA, without friction, with minimum values of friction and with maximum values of friction. The input is a road class C profile at 100 km/h

This demonstrates the importance of the translation–rotation factor (mm/rev), not only for the damping constant but also for its equivalent mass. The translation–rotation factor in the rotational EHSA is one of the main design parameters. The higher the factor, the voltage generation increases. However, the electromagnetic torque decreases and affects the damping force.

The results of the optimization are shown in Fig. 19. As can be seen, all variables improve with respect to their initial values. The comfort, which is represented as the average acceleration, improves 23.86% with respect to its initial value. The value of ground adhesion, which is represented as the mean relative displacement between the ground and the wheel, improves 26.91% with respect to its initial value. The average power generated goes from 100 to 162 W, and the efficiency goes from 36 to 81%.

Therefore, the optimized BS-EHSA remains as follows: since the optimum generator voltage constant has a value of 29.8 rpm/V, the Maxon 218014 will be used. The optimum total inertia is about 250 g cm^2; since the inertia of the selected motor is 118 g cm^2, a spindle must be produced for the BS-EHSA having an inertia of 132 g cm^2 and a screw lead of 7 mm/rev. Finally, a 75 Ω electrical resistance is connected to the BS-EHSA.

Using the optimized BS-EHSA, the influence of the friction parameters, found in Sect. 3, is evaluated using the following indicators: comfort, ground adhesion, power generation and energy efficiency. The results are shown in Fig. 20, in which each of these indicators at different vehicle speeds is reflected

To give a concrete example, when the vehicle moves at 100 km/h: firstly, comfort can deteriorate by 15%

Table 4 Influence of the friction in the parameters of: comfort, rode handling, power generated and efficiency

	Without friction	Min friction	Max friction
Comfort		+ 0.57%	− 15.01%
Road handling		+ 1.7%	+ 7.83%
Power generated	174.9 W	148.61 W	110.1 W
Efficiency	81%	67.58%	49.64%

compared to a frictionless BS-EHSA. However, the vehicle adhesion is favored at a higher friction value, increasing up to 8%. The efficiency of the system can be between 50 and 68%. As for the instant power generated, this can be reduced between 15 and 37%, as shown in Fig. 21 and Table 4. The mean power generated with the maximum values of friction is around 110 W with power peaks up to 580 W and with the minimum values of friction is 148 W with power peaks up to 710 W. It should be point out that at higher friction values the peak power decreases. This factor is important in the storage of the energy, concerning the life of the batteries and/or supercapacitors.

5 Conclusions

Energy-harvesting shock absorbers (EHSAs) have been introduced in the last decade as a viable technology for improving the performance and durability of electric and hybrid vehicles. However, in order to be able to ascertain the potential of his technology for specific applications and conditions, the computational models that are used must behave as close as possible to reality.

In the design of this kind of systems, one of the most important parameters is the friction between the moving parts. This paper has presented a method for the estimation of nonlinear friction parameters from tests and MOOP algorithms. Because an exact value for each friction parameter cannot be ensured, upper and lower boundaries have been established. This allows an analysis of the effect of the variation in these parameters within this range in the dynamics and energy efficiency of the vehicle.

For the purposes of this study, the analysis uses the BS-EHSA system and assesses how friction parameters can affect comfort, ground adhesion, power generation and energy efficiency. To achieve this, design parameters of the BS-EHSA have been optimized first, and then, their behavior has been compared with and without friction.

The friction parameters depend solely on the design and the way in which the device is manufactured. This article presented a prototype of the BS-EHSA system and the maximum and minimum friction values obtained from test results. This means that, using the estimated friction parameters, comfort can deteriorate by as much as 15%, the power generated can be between 110 and 174.9 W per damper, depending on the speed of the vehicle and the energy efficiency can be between 50 and 68%. On the other hand, the frictions can benefit from the vehicle adhesion by between 1.3 and 7.8%. The method for identifying the nonlinear friction parameters presented in this paper can be used to increase the validity of any other EHSA models based on different designs in order to obtain reliable results of the simulations regarding recovered power, damping, comfort and efficiency.

Compliance with ethical standards

Conflict of interest The authors declare that they have no conflict of interest.

References

1. Amati, N., Festini, A., Tonolii, A.: Design of electromagnetic shock absorbers for automotive suspensions. Veh. Syst. Dyn. **49**(12), 1913–1928 (2011)
2. Amatia, N., Canova, A., Cavalli, F., Carabelli, S., Festini, A., Tonoli, A., Caviasso, G.: Electromagnetic shock absorbers for automotive suspensions: Electromechanical design. In: ASME 8th Biennial Conference on Engineering Systems Design and Analysis (2006)
3. Benini, C., Gadola, M., Chindamo, D., Uberti, S., Marchesin, F.P., Barbosa, R.S.: The influence of suspension components friction on race car vertical dynamics. Veh. Syst. Dyn. **55**(3), 338–350 (2017). https://doi.org/10.1080/00423114.2016.1267370
4. Bowen, L., Vinolas, J., OLazagoitia, J.: Methodology for comparing the functional performance of energy harvesting shock absorbers. Int. J. Appl. Electromagn. Mech. **2017**, 545–564 (2017). https://doi.org/10.3233/JAE-170057
5. Bruni, S., Vinolas, J., Berg, M., Polach, O., Stichel, S.: Modelling of suspension components in a rail vehicle dynamics context. Veh. Syst. Dyn. **49**(7), 1021–1072 (2011). https://doi.org/10.1080/00423114.2011.586430
6. Erturk, A., Inman, D.: Broadband piezoelectric power generation on high-energy orbits of the bistable duffing oscillator with electromechanical coupling. J. Sound Vib.

330(10), 2339–2353 (2011). https://doi.org/10.1016/j.jsv.2010.11.018. (Dynamics of Vibro-Impact Systems)
7. Fang, Z., Guo, X., Xu, L., Zhang, H.: Experimental study of damping and energy regeneration characteristics of a hydraulic electromagnetic shock absorber. Adv. Mech. Eng. **5**, 943,528 (2013). https://doi.org/10.1155/2013/943528
8. Galluzzi, R., Tonoli, A., Amati, N., Curcuruto, G., Conti, P., Greco, G., Nepote, A.: Regenerative shock absorbers and the role of the motion rectifier. In: SAE technical paper. SAE International (2016). https://doi.org/10.4271/2016-01-1552
9. Gembicki, F., Haimes, Y.: Approach to performance and sensitivity multiobjective optimization: the goal attainment method. IEEE Trans. Autom. Control **20**(6), 769–771 (1975). https://doi.org/10.1109/TAC.1975.1101105
10. Guo, S., Liu, Y., Xu, L., Guo, X., Zuo, L.: Performance evaluation and parameter sensitivity of energy-harvesting shock absorbers on different vehicles. Veh. Syst. Dyn. **54**(7), 918–942 (2016)
11. Iwnicki, S.: Handbook of Railway Vehicle Dynamics. Taylor and Francis Group, Boca Raton (2006)
12. Kashani, H.: Analytical parametric study of bi-linear hysteretic model of dry friction under harmonic, impulse and random excitations. Nonlinear Dyn. **89**(1), 267–279 (2017). https://doi.org/10.1007/s11071-017-3452-y
13. Li, P., Zuo, L.: Influences of the electromagnetic regenerative dampers on the vehicle suspension performance. Proc. Inst. Mech. Eng. Part D J. Automob. Eng. **231**(3), 383–394 (2016)
14. Li, Z., Zuo, L., Kuang, J., George, L.: Energy-harvesting shock absorber with a mechanical motion rectifier. Smart Mater. Struct. **22**(2), 025008 (2013)
15. Li, Z., Zuo, L., Luhrs, G., Lin, L., Qin, Yx: Electromagnetic energy-harvesting shock absorbers: design, modeling, and road tests. IEEE Trans. Veh. Technol. **62**(3), 1065–1074 (2013)
16. Lin, X., Bo, Y., Xuexun, G., Jun, Y.: Simulation and performance evaluation of hydraulic transmission electromagnetic energy-regenerative active suspension. In: 2010 Second WRI Global Congress on Intelligent Systems, vol. 3, pp. 58–61 (2010). https://doi.org/10.1109/GCIS.2010.249
17. Liu, Y., Xu, L., Zuo, L.: Design, modeling, lab, and field tests of a mechanical-motion-rectifier-based energy harvester using a ball-screw mechanism. IEEE ASME Trans. Mechatron. **22**(5), 1933–1943 (2017)
18. Maravandi, A., Moallem, M.: Regenerative shock absorber using a two-leg motion conversion mechanism. IEEE ASME Trans. Mechatron. **20**(6), 2853–2861 (2015). https://doi.org/10.1109/TMECH.2015.2395437
19. Nagode, C., Ahmadian, M., Taherii, S.: Vibration-based energy harvesting systems for on-board applications. In: Joint Rail Conference (2011)
20. Oprea, R.A., Mihailescu, M., Chirila, A.I., Deaconu, I.D.: Design and efficiency of linear electromagnetic shock absorbers. In: 2012 13th International Conference on Optimization of Electrical and Electronic Equipment (OPTIM) (2012)
21. Peng, M., Guo, X., Zou, J., Zhang, C.: Simulation study on vehicle road performance with hydraulic electromagnetic energy-regenerative shock absorber. In: SAE technical paper. SAE International (2016). https://doi.org/10.4271/2016-01-1550
22. Popp, K.: Non-smooth mechanical systems—an overview. Forsch. Ing. **64**(9), 223 (1998). https://doi.org/10.1007/PL00010860
23. Popp, K., Hinrichs, N., Oestreich, M.: Dynamical behaviour of a friction oscillator with simultaneous self and external excitation. Sadhana **20**(2), 627–654 (1995). https://doi.org/10.1007/BF02823210
24. Sabzehgar, R., Maravandi, A., Moallem, M.: Energy regenerative suspension using an algebraic screw linkage mechanism. IEEE ASME Trans. Mechatron. **19**(4), 1251–1259 (2014). https://doi.org/10.1109/TMECH.2013.2277854
25. Vidmar, B.J., Feeny, B.F., Shaw, S.W., Haddow, A.G., Geist, B.K., Verhanovitz, N.J.: The effects of coulomb friction on the performance of centrifugal pendulum vibration absorbers. Nonlinear Dyn. **69**(1), 589–600 (2012). https://doi.org/10.1007/s11071-011-0289-7
26. Wei, C., Taghavifar, H.: A novel approach to energy harvesting from vehicle suspension system: half-vehicle model. Energy **134**, 279–288 (2017). https://doi.org/10.1016/j.energy.2017.06.034
27. Xie, X., Wang, Q.: Energy harvesting from a vehicle suspension system. Energy **86**, 385–392 (2015). https://doi.org/10.1016/j.energy.2015.04.009
28. Xuezheng, J., Wang, J., Yancheng, L., Jianchun, L.: Design and modelling of a novel linear electromagnetic vibration energy harvester. Int. J. Appl. Electromagn. Mech. **46**(1), 165–183 (2014)
29. Zhang, G., Cao, J., Yu, F.: Design of active and energy-regenerative controllers for dc-motor-based suspension. Mechatronics **22**(8), 1124–1134 (2012)
30. Zhang, X., Xu, J., Feng, Z.: Nonlinear equivalent model and its identification for a delayed absorber with magnetic action using distorted measurement. Nonlinear Dyn. **88**(2), 937–954 (2017). https://doi.org/10.1007/s11071-016-3286-z
31. Zhang, Y., Chen, H., Guo, K., Zhang, X., Li, S.E.: Electro-hydraulic damper for energy harvesting suspension: modeling, prototyping and experimental validation. Appl. Energy **199**, 1–12 (2017). https://doi.org/10.1016/j.apenergy.2017.04.085
32. Zhang, Y., Guo, K., Wang, D., Chen, C., Li, X.: Energy conversion mechanism and regenerative potential of vehicle suspensions. Energy **119**, 961–970 (2017). https://doi.org/10.1016/j.energy.2016.11.045
33. Zhang, Y., Zhang, X., Zhan, M., Guo, K., Zhao, F., Liu, Z.: Study on a novel hydraulic pumping regenerative suspension for vehicles. J. Frankl. Inst. **352**(2), 485–499 (2015). https://doi.org/10.1016/j.jfranklin.2014.06.005. (Special Issue on Control and Estimation of Electrified vehicles)
34. Zhang, Z., Zhang, X., Chen, W., Rasim, Y., Salman, W., Pan, H., Yuan, Y., Wang, C.: A high-efficiency energy regenerative shock absorber using supercapacitors for renewable energy applications in range extended electric vehicle. Appl. Energy **178**, 177–188 (2016). https://doi.org/10.1016/j.apenergy.2016.06.054
35. Zhu, H., Yang, J., Zhang, Y., Feng, X., Ma, Z.: Nonlinear dynamic model of air spring with a damper for vehicle ride comfort. Nonlinear Dyn. **89**(2), 1545–1568 (2017). https://doi.org/10.1007/s11071-017-3535-9

36. Zou, J., Guo, X., Xu, L., Gangfeng, T., Zhang, C., Zhang, J.: Design, modeling, and analysis of a novel hydraulic energy-regenerative shock absorber for vehicle suspension. Shock Vib. **2017**, 12 (2017). https://doi.org/10.1155/2017/3186584
37. Zuo, L., Nayfeh, S.: Low order continuous-time filters for approximation of the iso 2631-1 human vibration sensitivity weightings. J. Sound Vib. **265**(2), 459–465 (2003). https://doi.org/10.1016/S0022-460X(02)01567-5
38. Zuo, L., Scully, B., Shestani, J., Zhou, Y.: Design and characterization of an electromagnetic energy harvester for vehicle suspensions. Smart Mater. Struct. **19**(4), 045003 (2010)

Terms and Conditions

Springer Nature journal content, brought to you courtesy of Springer Nature Customer Service Center GmbH (“Springer Nature”).
Springer Nature supports a reasonable amount of sharing of research papers by authors, subscribers and authorised users (“Users”), for small-scale personal, non-commercial use provided that all copyright, trade and service marks and other proprietary notices are maintained. By accessing, sharing, receiving or otherwise using the Springer Nature journal content you agree to these terms of use (“Terms”). For these purposes, Springer Nature considers academic use (by researchers and students) to be non-commercial.
These Terms are supplementary and will apply in addition to any applicable website terms and conditions, a relevant site licence or a personal subscription. These Terms will prevail over any conflict or ambiguity with regards to the relevant terms, a site licence or a personal subscription (to the extent of the conflict or ambiguity only). For Creative Commons-licensed articles, the terms of the Creative Commons license used will apply.
We collect and use personal data to provide access to the Springer Nature journal content. We may also use these personal data internally within ResearchGate and Springer Nature and as agreed share it, in an anonymised way, for purposes of tracking, analysis and reporting. We will not otherwise disclose your personal data outside the ResearchGate or the Springer Nature group of companies unless we have your permission as detailed in the Privacy Policy.
While Users may use the Springer Nature journal content for small scale, personal non-commercial use, it is important to note that Users may not:

1. use such content for the purpose of providing other users with access on a regular or large scale basis or as a means to circumvent access control;
2. use such content where to do so would be considered a criminal or statutory offence in any jurisdiction, or gives rise to civil liability, or is otherwise unlawful;
3. falsely or misleadingly imply or suggest endorsement, approval , sponsorship, or association unless explicitly agreed to by Springer Nature in writing;
4. use bots or other automated methods to access the content or redirect messages
5. override any security feature or exclusionary protocol; or
6. share the content in order to create substitute for Springer Nature products or services or a systematic database of Springer Nature journal content.

In line with the restriction against commercial use, Springer Nature does not permit the creation of a product or service that creates revenue, royalties, rent or income from our content or its inclusion as part of a paid for service or for other commercial gain. Springer Nature journal content cannot be used for inter-library loans and librarians may not upload Springer Nature journal content on a large scale into their, or any other, institutional repository.
These terms of use are reviewed regularly and may be amended at any time. Springer Nature is not obligated to publish any information or content on this website and may remove it or features or functionality at our sole discretion, at any time with or without notice. Springer Nature may revoke this licence to you at any time and remove access to any copies of the Springer Nature journal content which have been saved.
To the fullest extent permitted by law, Springer Nature makes no warranties, representations or guarantees to Users, either express or implied with respect to the Springer nature journal content and all parties disclaim and waive any implied warranties or warranties imposed by law, including merchantability or fitness for any particular purpose.
Please note that these rights do not automatically extend to content, data or other material published by Springer Nature that may be licensed from third parties.
If you would like to use or distribute our Springer Nature journal content to a wider audience or on a regular basis or in any other manner not expressly permitted by these Terms, please contact Springer Nature at

onlineservice@springernature.com